

Generalizing to Unseen Domains in Diabetic Retinopathy with Disentangled Representations

Peng Xia^{1,2*}, Ming Hu^{1*}, Feilong Tang¹, Wenxue Li¹, Wenhao Zheng²,
Lie Ju¹, Peibo Duan¹, Huaxiu Yao²✉, and Zongyuan Ge¹✉

¹ Monash University, Melbourne, Victoria, Australia

² UNC-Chapel Hill, Chapel Hill, NC, USA

richard.peng.xia@gmail.com, huaxiu@cs.unc.edu, zongyuan.ge@monash.edu

Abstract. Diabetic Retinopathy (DR), induced by diabetes, poses a significant risk of visual impairment. Accurate and effective grading of DR aids in the treatment of this condition. Yet existing models experience notable performance degradation on unseen domains due to domain shifts. Previous methods address this issue by simulating domain style through simple visual transformation and mitigating domain noise via learning robust representations. However, domain shifts encompass more than image styles. They overlook biases caused by implicit factors such as ethnicity, age, and diagnostic criteria. In our work, we propose a novel framework where representations of paired data from different domains are decoupled into semantic features and domain noise. The resulting augmented representation comprises original retinal semantics and domain noise from other domains, aiming to generate enhanced representations aligned with real-world clinical needs, incorporating rich information from diverse domains. Subsequently, to improve the robustness of the decoupled representations, class and domain prototypes are employed to interpolate the disentangled representations while data-aware weights are designed to focus on rare classes and domains. Finally, we devise a robust pixel-level semantic alignment loss to align retinal semantics decoupled from features, maintaining a balance between intra-class diversity and dense class features. Experimental results on multiple benchmarks demonstrate the effectiveness of our method on unseen domains. The code implementations are accessible on <https://github.com/richard-peng-xia/DECO>.

Keywords: Diabetic Retinopathy · Domain Generalization · Disentangled Representations.

1 Introduction

Diabetic Retinopathy (DR) is a diabetes-induced ocular disorder that affects the retina, which epitomizes one of the foremost causes of blindness [25]. Typically, the diagnosis of DR is based on the presence of several key lesions, namely

* Equal Contribution

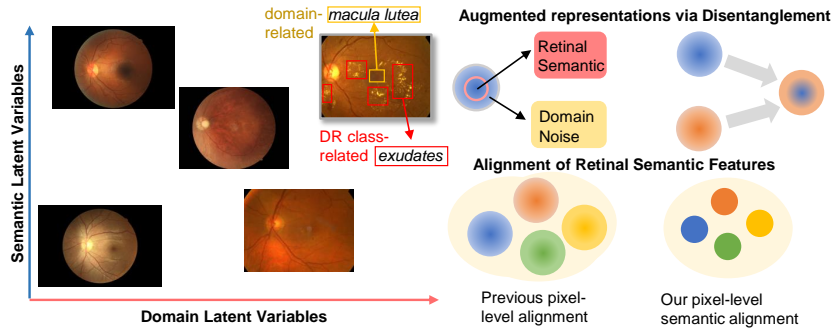


Fig. 1. (Left) An example of fundus-based domain variances. The horizontal distance represents domain differences, and the vertical distance denotes DR category differences. (Right) The motivations of our approach. Firstly, while the augmentation methods are simple visual transformations, we consider more feature-level class-agnostic latent noise, such as macular degeneration caused by age. Additionally, existing pixel-level alignment may act on features containing domain bias, replacing original features with decoupled semantic features to alleviate domain noise.

microaneurysms, hemorrhages, soft or hard exudates, hemorrhages, and cotton wool spots. Therefore, the grading of DR usually includes five categories: no DR, mild DR, moderate DR, severe DR, and proliferative DR [20].

Although deep learning methods have achieved promising results in grading DR [4,9,14,17], which simplifies the diagnostic process and reduces the demand for trained ophthalmologists, one major challenge they face in practical clinical applications is domain shifts [2,3,4,6], meaning there are some visual biases between training and testing data caused by factors such as imaging conditions or the ethnic of the population, as shown in Figure 1. This leads to a decline in models’ performance when these models are applied to new data from unseen domains, which is known as Domain Generalization (DG) [29,32,35,24].

Previous efforts have sought to learn robust domain-invariant representations, such as through flatness and regularization [2,33], and variational autoencoders [6]. There are works from the perspective of image augmentation [3,32,31], using visual transformation or image degradation to simulate domain shifts. However, generalized features are likely affected by domain biases unrelated to DR categories, such as macular degeneration in elderly retinas and ethnic variations in retinal structure. This renders current data augmentation schemes and direct feature learning ineffective when confronted with new unseen domains. Additionally, there are works proposing pixel-level supervised losses to learn diverse intra-class features [3], but the targets themselves contain domain noise, which makes the representations less robust.

Considering these drawbacks, we propose to **Decouple the rEpresentations of semantiC features from dOmain features** to reduce domain bias, which we call **DECO**. Specifically, features are decoupled into representations of semantic features (DR-related retinal semantics, *e.g.*, microaneurysms, hemorrhages,

hard/soft exudates) and domain features (domain noise, *e.g.*, explicit noise in image style and implicit noise stemming from age, gender, and ethnicity, etc.). To mitigate the impact of domain shifts, we average the domain information over examples of the same class and construct class prototype representations. Then we linearly interpolate each semantic representation using the corresponding class prototype. Similarly, we interpolate domain representations with class-agnostic domain factors to improve training stability and remove noise. During the insertion process, we design data-aware weights to focus on rare classes and domains. By utilizing a set of data from different domains, new representations containing the semantic features of one example and domain features from another can be reassembled for data augmentation. This approach can effectively improve the model’s generalization ability and allows for more targeted data sampling from the perspective of domain or class, especially for rare classes or domains, thus achieving overall performance stability. In Domain Generalization (DG), sufficient intra-class variability is crucial, a functionality not achievable through traditional image-level supervised losses. Therefore, in DR grading, the diverse diagnostic patterns across different domains encourage the model to learn retinal lesion semantics at the pixel level as extensively as possible, as pixel-level supervised representations are likely to be noisy, which is overlooked in prior works [3]. By introducing decoupled retinal semantics for pixel-level alignment alongside severity supervision at the image level, we encourage the model to learn features with adequate intra-class variability while preserving diagnostic patterns.

Our contributions can be summarized as: (1) We propose decoupling the representation of semantic features from domain features and utilizing a combination of semantic features and features from different domains for feature-level data augmentation. Moreover, to improve the robustness of the disentangled representations, class and domain prototypes are separately interpolated into their corresponding representations; (2) We design a robust pixel-level alignment loss to align retinal semantics decoupled from representations; (3) Extensive experiments on comprehensive benchmarks demonstrate the effectiveness of our framework on unseen domains.

2 Methodology

To achieve class-unbiased and domain-invariant representations, we propose DECO, outlined as shown in Figure 2. The key concept is to decouple retinal image representation into class-related retinal semantics and domain noise. DECO migrates domain noise to all instances, which offers greater adaptability compared to manually designed image augmentation methods [21,15]. Additionally, DECO averages the semantic representations of each category and domain noise separately to interpolate the representation of each instance. Finally, we extract retinal semantics from the features for further pixel-level alignment, enabling the model to learn robust class-related retinal features.

Task Settings. In DG, let $\mathcal{D} = \{D_1, \dots, D_S\}$ denote the source domains, where each domain D_i includes data triplets (x_i, y_i, d) representing input fundus image

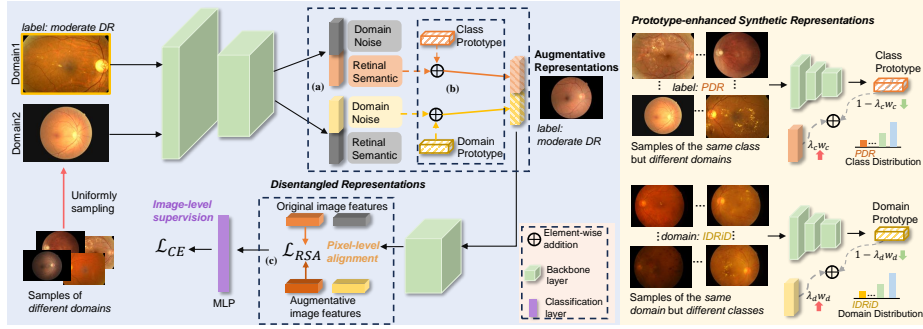


Fig. 2. The overview of our proposed method. (a) Representation decoupling and recombination. (b) Representation enhancement with class and domain prototypes. The specific process is shown in the right panel. (c) Robust pixel-level semantic alignment.

x_i , label y_i , and the domain d , drawn from the domain-specific distribution $P_i(x, y)$. For each domain d , we define the number of training examples in each class as $n_i = \{n_{d,1}, \dots, n_{d,C}\}$. The goal of DG is to learn a function $f: \mathcal{X} \rightarrow \mathcal{Y}$ that minimizes the expected loss over an unseen target domain D_T with its own unique distribution $P_T(x, y)$.

Decoupling and Recombination of Representations. DECO constructs augmented instances by combining the semantic representation of one instance with the domain noise of another, thereby recombining pairs of instances to augment instances of diverse styles. Inspired by style transfer [12], we employ instance normalization [22] to decouple semantic and domain noise. In an exemplar (x, y, d) , the hidden representation at the l -th ($l < L$) layer is denoted as $r = f^l(x) \in \mathbb{R}^{C \times H \times W}$, where C , H , and W signify the channel, height, and width dimensions, respectively. InstanceNorm normalizes it as:

$$z(r) = \text{InstanceNorm}(r) = \frac{r - \mu(r)}{\sigma(r)}. \quad (1)$$

where $\mu(\cdot)$, $\sigma(\cdot)$ are the mean and standard deviation computed across the spatial dimensions of r for each channel and each sample:

$$\mu(r) = \frac{1}{HW} \sum_{h=1}^H \sum_{w=1}^W r_{h,w}, \quad \sigma(r) = \sqrt{\frac{1}{HW} \sum_{h=1}^H \sum_{w=1}^W (r_{h,w} - \mu(r))^2}. \quad (2)$$

InstanceNorm occurs in feature space, where the affine parameters can alter the style of the image [12,22]. Therefore, we consider the normalized example $z(r)$ as the semantic representation, representing the retinal-related semantics in retinal images, while $\mu(r)$ and $\sigma(r)$ are regarded as domain noise, encompassing factors such as image style, background, ethnicity, and age differences.

After decoupling representations, an augmented representation is generated by interchanging semantic representations and domain noise within a pair of exam-

ples (x_i, y_i, d_i) and (x_j, y_j, d_j) .

$$r' = \sigma(r_i) \left(\frac{r_i - \mu(r_i)}{\sigma(r_i)} \right) + \mu(r_j), \quad \hat{y} = y_i. \quad (3)$$

Combining the semantic representation of x_i with the domain representation of x_j yields an augmented representation r' with the category y_i . By decoupling and recombining representations, numerous augmented representations can be generated, encompassing diverse domain noise, particularly making DECO more reliable when faced with domain or class imbalance.

Prototype-enhanced Synthetic Representations. Although instance normalization can effectively distinguish semantic information from domain noise, it is challenging to entirely shield the semantic information of each instance from domain bias. Therefore, to improve the robustness of semantic representations, we leverage the averaged semantic representations from the same class but different domains [27]. Considering the diversity of the same class, we balance class and domain invariance by combining corresponding class prototype representations and semantic representations. The class prototype representation p_c is an invariant representation belonging to class c , independent of the domain, obtained by averaging semantic representations of instances belonging to class c :

$$p_c = \frac{1}{n_{\star,c}} \sum_{i=1}^{n_{\star,c}} z(r_i) = \frac{1}{n_{\star,c}} \sum_{i=1}^{n_{\star,c}} \frac{r_i - \mu(r_i)}{\sigma(r_i)}, \quad \text{where } n_{\star,c} = \sum_{k=1}^S n_{k,c}. \quad (4)$$

For every instance (x, y, d) where $y = c$, the prototype-enhanced semantic representation $\hat{z}(r)$ is derived through the interpolation of $z(r)$ with the class prototype p_c . Additionally, considering the class imbalance [26,11], we design a class-aware weight with the interpolation coefficient λ_c to balance the semantic representations and prototypes of minority groups.

$$\hat{z}(r) = \lambda_c w_c z(r) + (1 - \lambda_c w_c) p_c, \quad w_c = \frac{\sum_{c=1}^C \sum_{k=1}^S (n_{k,c})^{\gamma_c}}{\sum_{k=1}^S (n_{k,c})^{\gamma_c}}, \quad (5)$$

where γ_c is a scale hyper-parameter to provide more flexibility. Similarly, in the ideal scenario, $\mu(r)$ and $\sigma(r)$ exclusively contain domain noise representations, yet they may also include class-related representations, such as certain subtle lesions. In this case, we obtain domain prototype representations u_d and v_d by averaging examples from different classes within the same domain to alleviate semantic information:

$$u_d = \frac{1}{n_{d,\star}} \sum_{i=1}^{n_{d,\star}} \mu(r_i), \quad v_d = \frac{1}{n_{d,\star}} \sum_{i=1}^{n_{d,\star}} \sigma(r_i), \quad \text{where } n_{d,\star} = \sum_{k=1}^C n_{d,k}. \quad (6)$$

Then, we design a weighting scheme tailored to domains with inadequate representation, followed by interpolating the domain noise of each instance with domain prototypes using domain weights and a balancing coefficient:

$$\hat{\mu}(r) = \lambda_d w_d \mu(r) + (1 - \lambda_d w_d) u_d, \quad \hat{\sigma}(r) = \lambda_d w_d \sigma(r) + (1 - \lambda_d w_d) v_d, \quad (7)$$

Table 1. Comparison with state-of-the-art approaches under the DG test.

Target	APTOS			DeepDR			FGADR			IDRID			Messidor			RLDR			Average		
Metrics	AUC	ACC	F1	AUC	ACC	F1	AUC	ACC	F1	AUC	ACC	F1	AUC	ACC	F1	AUC	ACC	F1	AUC	ACC	F1
ERM	75.0	44.4	38.9	77.0	39.5	34.3	66.2	32.0	27.1	82.3	50.0	44.1	79.1	60.7	43.4	75.9	36.5	35.7	75.9	43.8	37.3
Mixup [34]	75.3	62.6	43.2	75.3	29.0	25.2	66.7	42.3	32.3	78.8	39.0	27.6	76.7	54.7	32.6	76.9	43.6	37.7	75.0	45.2	33.1
MixStyle [37]	79.0	65.8	39.9	76.9	32.9	27.9	71.2	35.8	22.7	83.0	51.4	39.2	75.2	62.2	36.5	75.5	41.1	31.4	76.8	48.2	32.9
GREEN [17]	75.1	53.8	38.9	76.4	28.1	24.9	69.5	41.3	31.5	79.9	41.3	32.2	75.8	52.0	36.8	74.8	34.0	34.4	75.3	41.8	33.1
CABNet [9]	75.8	55.5	39.4	75.2	42.7	31.8	73.2	43.7	34.8	79.2	44.8	37.3	74.2	56.1	34.1	75.8	37.0	35.6	75.6	46.6	35.5
DDAIG [36]	78.0	67.1	41.0	75.6	37.6	32.2	73.6	42.0	33.8	82.1	37.4	27.0	76.6	58.4	35.3	75.6	36.1	27.7	76.9	46.4	32.8
ATS [28]	77.1	56.9	38.3	79.4	36.1	31.6	74.7	46.7	33.4	83.0	41.5	34.9	77.2	64.7	35.8	76.5	37.4	34.9	78.0	47.2	34.8
Fishr [19]	79.2	66.6	43.4	81.1	48.1	34.4	73.3	44.4	34.4	82.7	40.3	27.6	76.4	65.1	41.1	77.4	36.8	34.7	78.4	50.2	35.9
MDLT [30]	77.3	57.2	41.5	80.0	39.5	36.2	74.1	45.7	29.0	81.5	44.2	35.4	75.4	58.9	36.9	75.7	37.6	35.0	77.3	47.2	35.7
DRGen [2]	79.9	58.1	40.2	83.0	38.7	34.1	69.4	41.7	24.7	84.7	44.6	37.4	79.0	60.1	40.5	79.5	43.1	37.0	79.3	47.7	37.3
VAE-DG [6]	79.5	66.7	45.5	82.9	38.1	34.3	75.8	44.8	36.4	83.6	41.7	35.6	78.7	59.5	40.2	78.8	41.3	35.9	79.9	48.7	38.0
GDRNet [3]	79.9	66.8	46.0	84.7	53.1	45.3	80.8	45.3	39.4	84.0	40.3	35.9	83.2	63.4	50.9	82.9	45.8	43.5	82.6	52.5	43.5
DECO(Ours)	81.0	72.4	56.6	86.3	57.3	52.6	81.3	49.1	43.5	87.0	44.6	37.4	82.9	65.1	52.7	83.5	48.0	46.3	83.7	56.1	48.2

where $w_d = \frac{\sum_{d=1}^S \sum_{k=1}^C (n_{d,k})^{\gamma_d}}{\sum_{k=1}^C (n_{d,k})^{\gamma_d}}$. Finally, by replacing the original semantic representation and domain noise, the prototype-enhanced augmented representation:

$$\hat{r}' = \hat{\sigma}(r_j)\hat{z}(r_i) + \hat{\mu}(r_j), \quad \hat{y}' = y_i. \quad (8)$$

Robust Pixel-level Semantic Alignment Loss. Image-level supervised losses (such as cross-entropy) have been the most common, capable of learning dense class features. However, sufficient intra-class variation is crucial for domain generalization, with some works [3,5] proposing to encourage models to learn pixel-level supervision. However, they overlook that the representations for alignment are susceptible to domain interference. Therefore, we introduce decoupled retinal semantics for pixel-level alignment, along with image-level severity supervision, to encourage the model to learn robust class features on the retina while possessing features with sufficient intra-class variation. For each instance (x, y, d) , the original features are $r = f^L(x)$, and its augmented features are \hat{r}' . Our training objective combines \mathcal{L}_{img} and \mathcal{L}_{pixel} as follows:

$$\mathcal{L}_{total} = \mathcal{L}_{CE}(\text{MLP}(\hat{r}'), y) - \alpha \log \frac{\exp(z(\hat{r}') \cdot z(r)/\tau)}{\sum_{k=1}^{2M} \mathbf{1}_{[k \neq i]} \exp(z(\hat{r}') \cdot z(r_k)/\tau)}, \quad (9)$$

where $z(\cdot)$ represents semantic features, $\mathbf{1}_{[k \neq i]} \in \{0, 1\}$ is an indicator function that equals 1 when $k \neq i$, τ denotes the temperature parameter, α dynamically controls the task weight and M is the size of the randomly sampled mini-batch.

3 Experiments

Datasets and Metrics. We conduct a comprehensive evaluation of our method on GDRBench [3], which involves two generalization ability evaluation settings and eight popular public datasets. First, GDRBench adopts the classic leave-one-domain-out protocol (DG test), which requires leaving one domain for evaluation and training models on the rest. It involves six datasets, including DeepDR [16], Messidor [1], IDRID [18], APTOS [13], FGADR [38], and RLDR [23]. Additionally, it incorporates an extreme single-domain generalization setup (ESDG test), following the train-on-single-domain protocol on the above datasets for

Table 2. Comparison with state-of-the-art approaches under the ESDG test.

Source	APTOS			DeepDR			FGADR			IDRID			Messidor			RLDR			Average		
Metrics	AUC	ACC	F1	AUC	ACC	F1	AUC	ACC	F1	AUC	ACC	F1	AUC	ACC	F1	AUC	ACC	F1	AUC	ACC	F1
ERM	66.4	53.2	31.6	70.7	47.3	31.2	55.3	5.6	7.1	69.6	56.5	33.9	70.6	51.3	33.7	70.1	27.3	26.4	67.1	40.2	27.3
Mixup [34]	65.5	49.4	30.2	70.7	49.7	33.3	58.8	5.8	7.4	70.2	64.0	32.6	71.5	63.0	32.6	72.9	27.7	27.0	68.3	43.3	27.2
MixStyle [37]	62.0	48.8	25.0	53.3	32.0	14.6	51.0	7.0	7.9	53.0	53.5	19.4	51.4	57.6	16.8	53.5	18.3	6.4	54.0	36.2	15.0
GREEN [17]	67.5	52.6	33.3	71.2	44.6	31.1	58.1	5.7	6.9	68.5	60.7	33.0	71.3	54.5	33.1	71.0	31.9	27.8	67.9	41.7	27.5
CABNet [9]	67.3	52.2	30.8	70.0	55.4	32.0	57.1	6.1	7.5	67.4	62.7	31.7	72.3	63.8	35.3	75.2	23.0	25.4	68.2	43.8	27.2
DDAIG [36]	67.4	48.7	31.6	73.2	38.5	29.7	59.9	5.0	5.5	70.2	60.2	33.4	73.5	69.1	35.6	74.4	25.4	23.5	69.8	41.2	26.7
ATS [28]	68.8	51.7	32.4	72.7	52.4	33.5	60.3	5.3	5.7	69.1	66.6	30.6	73.4	64.8	32.4	75.0	24.2	23.9	69.9	44.2	26.4
Fishr [19]	64.5	61.7	31.0	72.1	61.0	30.1	56.3	6.0	7.2	71.8	48.0	30.6	74.3	52.0	33.8	78.6	19.3	21.3	69.6	41.3	25.7
MDLT [30]	67.6	53.3	32.4	73.1	50.2	33.7	57.1	7.1	7.8	71.9	61.7	32.4	73.4	58.9	34.1	76.6	29.0	30.0	70.0	43.4	28.4
DRGen [2]	69.4	60.7	35.7	78.5	39.4	31.6	59.8	6.8	8.4	70.8	67.7	30.6	77.0	64.5	37.4	78.9	19.0	21.2	72.4	43.0	27.5
VAE-DG [6]	67.7	51.9	32.3	75.4	53.6	33.4	60.2	5.1	5.6	72.4	63.0	32.3	75.8	59.9	35.7	78.9	23.6	24.0	71.7	42.9	27.2
GDRNet [3]	69.8	52.8	35.2	76.1	40.0	35.0	63.7	7.5	9.2	72.9	70.0	35.1	78.1	65.7	40.5	79.7	44.3	37.9	73.4	46.7	32.2
DECO(Ours)	70.6	59.7	36.4	78.2	40.3	35.8	65.5	9.9	11.7	74.2	74.8	38.7	79.8	70.1	44.9	81.1	49.3	40.8	75.0	50.7	34.7

training, but with two extra large-scale datasets, DDR [14] and EyePACS [8] for evaluation.

For evaluation, we report three critical metrics, namely accuracy (ACC), the area under the ROC curve (AUC), and macro F1-score (F1).

Implementation Details. We used ResNet-50 [10] pre-trained on ImageNet [7] as the backbone and a fully connected layer as the linear classifier. We use the AdamW optimizer with a learning rate of 5×10^{-4} , weight decay of 10^{-4} and a batch size of 32. The model is trained for 100 epochs. In our experiments, we apply cross-validation to tune all hyperparameters with grid search.

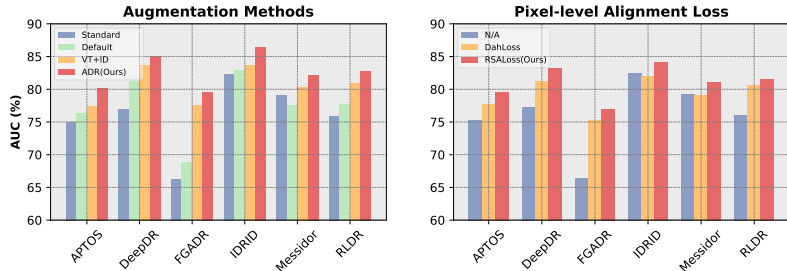
Baselines. Following [3], our comparative algorithms, besides the naive Empirical Risk Minimization (ERM), are mainly divided into three categories: conventional DR classification algorithms [9,17], domain generalization techniques [2,34,36,37,28,6], and feature representation methods [30,19].

Comparison with SoTA methods under the DG test. Table 1 demonstrates that our approach consistently outperforms previous state-of-the-art methods across all datasets. Furthermore, notable improvements are observed, particularly in domains with limited representation such as IDRiD, indicating the efficacy of our method in clinical applications. The decoupled feature enhancement and semantic alignment exhibit outstanding performance in scenarios with limited samples. Traditional DR classification methods, which do not account for domain shifts, exhibit weak generalization. In contrast, domain generalization and feature representation methods show improvements over the baseline, attributed to the strategic design addressing domain shifts. In summary, DECO significantly outperforms these SoTA methods. The decoupling representations effectively achieve feature-level data augmentation, while the incorporation of class or domain prototypes further enhances the robustness of augmented data. Additionally, robust pixel-level semantic alignment enables the model to learn precise intra-class variations, thereby improving model generalization.

Generalization from a single source domain. We further comprehensively evaluate the generalization performance by training on single-domain datasets and testing on large-scale unseen datasets. The results, as shown in Table 2, indicate a significant performance decrease for all methods, highlighting the challenge of the task. Despite the decreased utilization of feature-level data aug-

Table 3. Ablation studies on proposed components under the DG test.

ADR	Prototype	\mathcal{L}_{pixel}	APTOS	DeepDR	FGADR	IDRID	Messidor	RLDR	Average
-	-	-	75.26	77.21	66.35	82.44	79.29	75.95	76.08
✓	-	-	78.91	84.20	78.17	84.33	80.95	81.56	81.35
-	-	✓	79.53	83.16	76.99	84.05	81.02	81.64	81.07
✓	✓	-	80.15	85.13	79.56	86.37	82.11	82.84	82.69
✓	-	✓	80.28	85.40	79.83	86.30	82.43	82.96	82.87
✓	✓	✓	81.03	86.29	81.26	86.99	82.94	83.50	83.67

**Fig. 3.** Analysis of augmentation methods and \mathcal{L}_{pixel} under the DG test.

mentation in the ESDG test, DECO still outperforms other methods on most datasets due to its enhanced diversity within the same class samples and the learned robust domain-invariant representations.

Ablation study on the components. In Table 3, we conduct an ablation analysis on the three components. Firstly, the Augmented Disentangled Representations (ADR) significantly improve the model’s generalization ability. Subsequently, under the joint influence of class and domain prototypes, more robust augmented representations further optimize the model. Finally, robust pixel-level semantic alignment (RSALoss) of the disentangled semantic representations enhances the model’s generalization by improving robust intra-class diversity.

Further analysis of augmented methods and \mathcal{L}_{pixel} . To further analyze the effectiveness of ADR and RSALoss, the primary components of our approach, we compared them with state-of-the-art techniques in the same category. For the augmentation methods, the comparative methods included the standard DG augmentation [30], the default augmentation strategy in DRGen [2], visual transformation and image degradation [3]. Our proposed disentangled representation augmentation significantly outperforms the other methods. Regarding semantic alignment loss, we compared models without semantic alignment loss and with DahLoss [3]. Due to the improved robustness of alignment features with decoupled semantic representations, RSALoss demonstrates significant advantages.

4 Conclusion

In this work, we mitigate the performance gap faced by DR grading models due to domain shifts with disentangled representations. We innovatively propose a method to combine semantic representations relevant to DR classes with

domain noise from another domain. It enhances the model’s generalization to unseen domains. Then, to improve the robustness of decoupled representations, we derive prototypes by averaging class and domain representations and designing data-aware coefficients to adjust focus on different classes/domains, facilitating interpolation between semantic representations and prototypes. Finally, we introduce a robust pixel-level semantic alignment loss to simultaneously learn densely packed class features while preserving inter-class diversity.

References

1. Abràmoff, M.D., Lou, Y., Erginay, A., Clarida, W., Amelon, R., Folk, J.C., Niemeijer, M.: Improved automated detection of diabetic retinopathy on a publicly available dataset through integration of deep learning. *Investigative ophthalmology & visual science* **57**(13), 5200–5206 (2016)
2. Atwany, M., Yaqub, M.: Drgen: Domain generalization in diabetic retinopathy classification. In: *International Conference on Medical Image Computing and Computer-Assisted Intervention*. pp. 635–644. Springer (2022)
3. Che, H., Cheng, Y., Jin, H., Chen, H.: Towards generalizable diabetic retinopathy grading in unseen domains. In: *International Conference on Medical Image Computing and Computer-Assisted Intervention*. pp. 430–440. Springer (2023)
4. Che, H., Jin, H., Chen, H.: Learning robust representation for joint grading of ophthalmic diseases via adaptive curriculum and feature disentanglement. In: *International Conference on Medical Image Computing and Computer-Assisted Intervention*. pp. 523–533. Springer (2022)
5. Chen, T., Kornblith, S., Norouzi, M., Hinton, G.: A simple framework for contrastive learning of visual representations. In: *International conference on machine learning*. pp. 1597–1607. PMLR (2020)
6. Chokuwa, S., Khan, M.H.: Generalizing across domains in diabetic retinopathy via variational autoencoders. In: *International Conference on Medical Image Computing and Computer-Assisted Intervention*. pp. 265–274. Springer (2023)
7. Deng, J., Dong, W., Socher, R., Li, L.J., Li, K., Fei-Fei, L.: Imagenet: A large-scale hierarchical image database. In: *2009 IEEE conference on computer vision and pattern recognition*. pp. 248–255. Ieee (2009)
8. Emma, D., Jared, J., Will, C.: Eyepacs: Diabetic retinopathy detection (2015), <https://www.kaggle.com/competitions/diabetic-retinopathy-detection>
9. He, A., Li, T., Li, N., Wang, K., Fu, H.: Cabnet: Category attention block for imbalanced diabetic retinopathy grading. *IEEE Transactions on Medical Imaging* **40**(1), 143–153 (2020)
10. He, K., Zhang, X., Ren, S., Sun, J.: Deep residual learning for image recognition. In: *Proceedings of the IEEE conference on computer vision and pattern recognition*. pp. 770–778 (2016)
11. Hu, M., Wang, L., Yan, S., Ma, D., Ren, Q., Xia, P., Feng, W., Duan, P., Ju, L., Ge, Z.: Nurvid: A large expert-level video database for nursing procedure activity understanding. In: *Thirty-seventh Conference on Neural Information Processing Systems Datasets and Benchmarks Track* (2023)
12. Huang, X., Belongie, S.: Arbitrary style transfer in real-time with adaptive instance normalization. In: *Proceedings of the IEEE international conference on computer vision*. pp. 1501–1510 (2017)

13. Karthick, M., Sohler, D.: Aptos 2019 blindness detection (2019), <https://kaggle.com/competitions/aptos2019-blindness-detection>
14. Li, T., Gao, Y., Wang, K., Guo, S., Liu, H., Kang, H.: Diagnostic assessment of deep learning algorithms for diabetic retinopathy screening. *Information Sciences* **501**, 511–522 (2019)
15. Liu, H., Li, H., Wang, X., Li, H., Ou, M., Hao, L., Hu, Y., Liu, J.: Understanding how fundus image quality degradation affects cnn-based diagnosis. In: 2022 44th Annual International Conference of the IEEE Engineering in Medicine & Biology Society (EMBC). pp. 438–442. IEEE (2022)
16. Liu, R., Wang, X., Wu, Q., Dai, L., Fang, X., Yan, T., Son, J., Tang, S., Li, J., Gao, Z., et al.: Deepdrid: Diabetic retinopathy—grading and image quality estimation challenge. *Patterns* **3**(6) (2022)
17. Liu, S., Gong, L., Ma, K., Zheng, Y.: Green: a graph residual re-ranking network for grading diabetic retinopathy. In: Medical Image Computing and Computer Assisted Intervention—MICCAI 2020: 23rd International Conference, Lima, Peru, October 4–8, 2020, Proceedings, Part V 23. pp. 585–594. Springer (2020)
18. Porwal, P., Pachade, S., Kamble, R., Kokare, M., Deshmukh, G., Sahasrabudde, V., Meriaudeau, F.: Indian diabetic retinopathy image dataset (idrid): a database for diabetic retinopathy screening research. *Data* **3**(3), 25 (2018)
19. Rame, A., Dancette, C., Cord, M.: Fishr: Invariant gradient variances for out-of-distribution generalization. In: International Conference on Machine Learning. pp. 18347–18377. PMLR (2022)
20. Sebastian, A., Elharrouss, O., Al-Maadeed, S., Almaadeed, N.: A survey on deep-learning-based diabetic retinopathy classification. *Diagnostics* **13**(3), 345 (2023)
21. Shen, Z., Fu, H., Shen, J., Shao, L.: Modeling and enhancing low-quality retinal fundus images. *IEEE transactions on medical imaging* **40**(3), 996–1006 (2020)
22. Ulyanov, D., Vedaldi, A., Lempitsky, V.: Instance normalization: The missing ingredient for fast stylization. arXiv preprint arXiv:1607.08022 (2016)
23. Wei, Q., Li, X., Yu, W., Zhang, X., Zhang, Y., Hu, B., Mo, B., Gong, D., Chen, N., Ding, D., et al.: Learn to segment retinal lesions and beyond. In: 2020 25th International Conference on Pattern Recognition (ICPR). pp. 7403–7410. IEEE (2021)
24. Wu, Z., Yao, H., Liebovitz, D., Sun, J.: An iterative self-learning framework for medical domain generalization. *Advances in Neural Information Processing Systems* **36** (2024)
25. Wykoff, C.C., Khurana, R.N., Nguyen, Q.D., Kelly, S.P., Lum, F., Hall, R., Abbass, I.M., Abolian, A.M., Stoilov, I., To, T.M., et al.: Risk of blindness among patients with diabetes and newly diagnosed diabetic retinopathy. *Diabetes care* **44**(3), 748–756 (2021)
26. Xia, P., Xu, D., Ju, L., Hu, M., Chen, J., Ge, Z.: Lmpt: Prompt tuning with class-specific embedding loss for long-tailed multi-label visual recognition. arXiv preprint arXiv:2305.04536 (2023)
27. Xia, P., Yu, X., Hu, M., Ju, L., Wang, Z., Duan, P., Ge, Z.: Hgclip: Exploring vision-language models with graph representations for hierarchical understanding. arXiv preprint arXiv:2311.14064 (2023)
28. Yang, F.E., Cheng, Y.C., Shiau, Z.Y., Wang, Y.C.F.: Adversarial teacher-student representation learning for domain generalization. *Advances in Neural Information Processing Systems* **34**, 19448–19460 (2021)
29. Yang, X., Yao, H., Zhou, A., Finn, C.: Multi-domain long-tailed learning by augmenting disentangled representations. arXiv preprint arXiv:2210.14358 (2022)

30. Yang, Y., Wang, H., Katabi, D.: On multi-domain long-tailed recognition, imbalanced domain generalization and beyond. In: European Conference on Computer Vision. pp. 57–75. Springer (2022)
31. Yao, H., Wang, Y., Zhang, L., Zou, J.Y., Finn, C.: C-mixup: Improving generalization in regression. *Advances in neural information processing systems* **35**, 3361–3376 (2022)
32. Yao, H., Wang, Y., Li, S., Zhang, L., Liang, W., Zou, J., Finn, C.: Improving out-of-distribution robustness via selective augmentation. In: International Conference on Machine Learning. pp. 25407–25437. PMLR (2022)
33. Yao, H., Yang, X., Pan, X., Liu, S., Koh, P.W., Finn, C.: Improving out-of-domain generalization with domain relations. In: The Twelfth International Conference on Learning Representations (2023)
34. Zhang, H., Cisse, M., Dauphin, Y.N., Lopez-Paz, D.: mixup: Beyond empirical risk minimization. In: International Conference on Learning Representations (2018)
35. Zhou, K., Liu, Z., Qiao, Y., Xiang, T., Loy, C.C.: Domain generalization: A survey. *IEEE Transactions on Pattern Analysis and Machine Intelligence* (2022)
36. Zhou, K., Yang, Y., Hospedales, T., Xiang, T.: Deep domain-adversarial image generation for domain generalisation. In: Proceedings of the AAAI conference on artificial intelligence. vol. 34, pp. 13025–13032 (2020)
37. Zhou, K., Yang, Y., Qiao, Y., Xiang, T.: Domain generalization with mixstyle. In: International Conference on Learning Representations (2020)
38. Zhou, Y., Wang, B., Huang, L., Cui, S., Shao, L.: A benchmark for studying diabetic retinopathy: segmentation, grading, and transferability. *IEEE Transactions on Medical Imaging* **40**(3), 818–828 (2020)

Appendix for "Generalizing to Unseen Domains in Diabetic Retinopathy with Disentangled Representations"

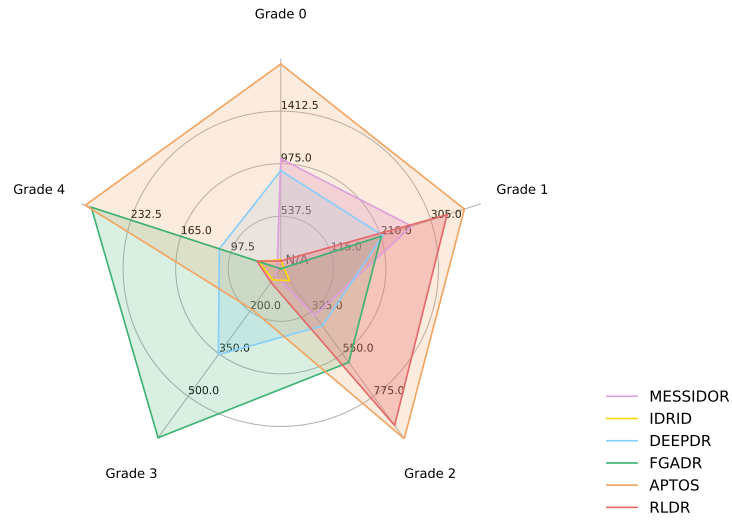


Fig. 4. Data distribution for each category in 6 datasets.

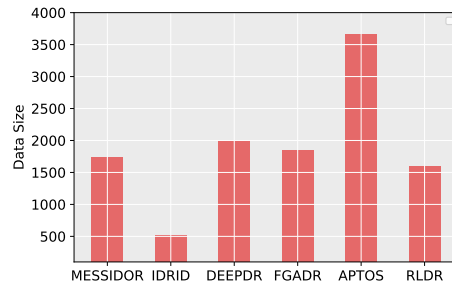


Fig. 5. Distribution of individual datasets.

Table 4. Hyperparameters for experiments. [†] denotes we adopt a warm start strategy of running vanilla ERM for the first few epochs to ensure reliable disentanglement. Interpolation coefficient $\lambda_c \sim \text{Beta}(\alpha_c, \alpha_c)$ and $\lambda_d \sim \text{Beta}(\alpha_d, \alpha_d)$.

Hyperparameters	DECO (DG)	DECO (ESDG)	Comparison methods
Epochs	100	100	100
Learning Rate	5×10^{-4}	5×10^{-4}	5×10^{-4}
Weight Decay	10^{-4}	10^{-4}	10^{-4}
Batch Size	32	32	32
Warm Start Epochs [†]	30	35	-
Class Prototype Mixup Parameter α_c	0.5	0.55	-
Domain Prototype Mixup Parameter α_d	0.5	0.4	-
γ_c	0.2	0.2	-
γ_d	0.2	-	-

Appendix for "Generalizing to Unseen Domains in Diabetic Retinopathy with Disentangled Representations"

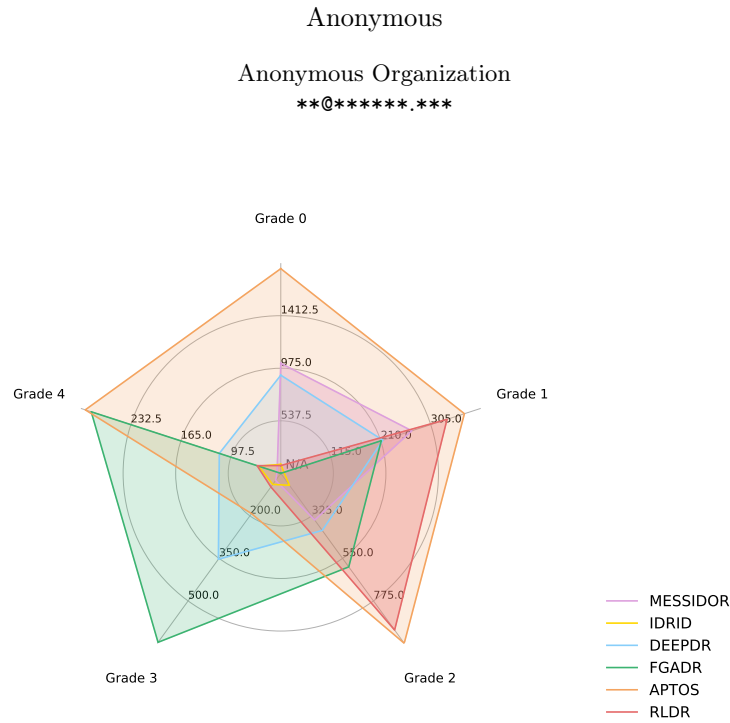


Fig. 1: Data distribution for each category in 6 datasets.

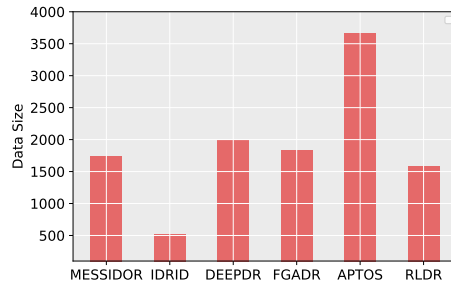


Fig. 2: Distribution of individual datasets.

Hyperparameters	GDRNet (DG)	GDRNet (ESDG)	Comparison methods
Epochs	100	100	100
Learning Rate	5×10^{-4}	5×10^{-4}	5×10^{-4}
Weight Decay	10^{-4}	10^{-4}	10^{-4}
Batch Size	32	32	32
Warm Start Epochs [†]	30	35	-
Class Prototype Mixup Parameter α_c	0.5	0.55	-
Domain Prototype Mixup Parameter α_d	0.5	0.4	-
γ_c	0.2	0.2	-
γ_d	0.2	-	-

Table 1: Hyperparameters for experiments. [†] denotes we adopt a warm start strategy of running vanilla ERM for the first few epochs to ensure reliable disentanglement. Interpolation coefficient $\lambda_c \sim \text{Beta}(\alpha_c, \alpha_c)$ and $\lambda_d \sim \text{Beta}(\alpha_d, \alpha_d)$.